

Surface Preparation and Thermal Spray in a Single Step: The PROTAL Process—Example of Application for an Aluminum-Base Substrate

C. Coddet, G. Montavon, S. Ayrault-Costil, O. Freneaux, F. Rigolet, G. Barbezat, F. Folio, A. Diard, and P. Wazen

(Submitted 3 August 1998; in revised form 8 January 1999)

Thermal spray techniques can fulfill numerous industrial applications. Coatings are thus applied to resist wear and corrosion or to modify the surface characteristics of the substrate (e.g., thermal conductivity/thermal insulation). However, many of these applications remain inhibited by some deposit characteristics, such as a limited coating adhesion or pores or by industrial costs because several nonsynchronized and sequential steps (that is, degreasing, sand blasting, and spraying) are needed to manufacture a deposit. The PROTAL process was designed to reduce the aforementioned difficulties by implementing simultaneously a Q-switched laser and a thermal spray torch. The laser irradiation is primarily aimed to eliminate the contamination films and oxide layers, to generate a surface state enhancing the deposit adhesion, and to limit the contamination of the deposited layers by condensed vapors. From PROTAL arises the possibility to reduce, indeed suppress, the preliminary steps of degreasing and grit blasting. In this study, the benefits of the PROTAL process were investigated, comparing adhesion of different atmospheric plasma spray coatings (e.g., metallic and ceramic coatings) on an aluminum-base substrate. Substrates were coated rough from the machine shop, for example, manipulated barehanded and without any prior surface preparation. Results obtained this way were compared with those obtained using a classical procedure; that is, degreasing and grit blasting prior to the coating deposition.

Keywords aluminum, coating adhesion, laser ablation, laser surface treatment, PROTAL, surface preparation

1. Introduction

Surface preparation prior to thermal spraying is a key step to ensure good adhesion of the coating. Usually, two successive stages are implemented: surface degreasing and surface roughening using, generally, grit blasting. Surface degreasing removes substances that taint surfaces, such as greases and oils (Ref 1). To achieve this step, solvent degreasing is commonly used, but the nature of the solvent needs to be well adapted to the nature of the material to be cleaned. Two major disadvantages are associated with surface degreasing: solvents and/or other chemicals have to be removed and recycled, and the operators as well as the environment have to be protected.

The major reason for grit blasting before thermal spraying is to generate sufficient surface roughness to ensure a mechanical anchoring between the coating and the substrate. However, grit blasting always leaves contamination (e.g., grit residue) entrapped in the material (Ref 2), the amount being higher when

the substrate is ductile (e.g., light weight alloys). These residues weaken the coating adhesion; decrease the fatigue properties of the substrate, especially for titanium and titanium-base alloys (Ref 3-4); limit the diffusion between the substrate and the deposit when applicable; and modify the wettability of the impinging particles onto the surface and induce thermal stresses due to thermal expansion coefficient mismatch between the grit media and the substrate. To bypass such disadvantages, surface roughening using water jets (Ref 5-6), acid pickling (Ref 7), electric discharge machining (Ref 8), and ice blasting have been tested. These operations are often expensive, though, and the steps of surface preparation and spraying remain sequential.

C. Coddet, G. Montavon, and S. Ayrault-Costil, Laboratoire d'Études et de Recherches sur les Matériaux et les Propriétés de Surface, Institut Polytechnique de Sévenans, BP 449, 90 010, Belfort Cedex, France; O. Freneaux and F. Rigolet, IREPA Laser, Parc d'Innovation, 67 400 Illkirch, Strasbourg, France; G. Barbezat, Sulzer-Metco AG, Rigackerstrasse 16, 5160, Wohlen, Switzerland; F. Folio, École Polytechnique Fédérale de Lausanne, CTML, CPMO, 1015, Lausanne, Switzerland; and A. Diard and P. Wazen, QUANTEL, Avenue de l'Atlantique, BP 23, 91 941 Les Ulis, Cedex, France. Contact e-mail: christian.coddet@utbm.fr.

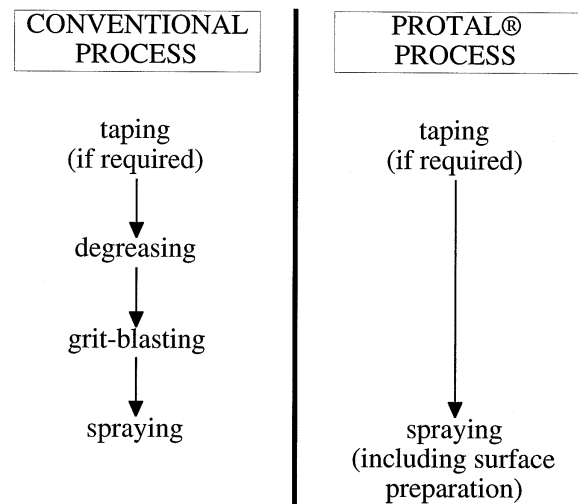


Fig. 1 Conventional versus PROTAL operating chart

With respect to these aspects of thermal spray processes, this article presents a new technique for surface preparation that can reduce the aforementioned difficulties by coupling a Q-switched Nd:YAG laser to the thermal spray torch. This process, named PROTAL (Ref 9-10), combines in a single step the spraying operation and the surface preparation (Fig. 1). The purpose of the laser irradiation is to eliminate the contamination films and oxide layers, to generate a surface state enhancing the deposit adhesion, and to limit the recontamination of the deposited layers by condensed vapors. The PROTAL process refers to a technique that allows simultaneous surface preparation and coating operation. This is obtained by the association of the spray gun with a specific laser gun (Fig. 2). The geometric ar-

range between both guns is achieved in such a way that the laser treatment precedes immediately or even overlaps the thermal deposition stage. Hence, the molten particles impinge onto a surface free of oxides and pollutants (e.g., condensed vapors, deposited dusts, etc.).

2. Physical Phenomena Occurring during Laser Ablation

2.1 Interaction between a Laser Beam and Matter

The surface of a solid may be in contact with a vacuum, a gas, a liquid, or another solid. When a surface is in contact with a gas,

Table 1 Physical, thermal, and optical characteristics of 2017 (aluminum-base) and Ti-6Al-4V (titanium-base) alloys

Properties	2017 aluminum-base alloy	Reference No.	Ti-6Al-4V titanium-base alloy	Reference No.
Melting temperature, °C	660	20	1600	20
	512-641	21	1650	21
Thermal conductivity, $W \cdot m^{-1} \cdot K^{-1}$	300	20	30	20
	238	14	20.7	14
	193	21		
Absorption depth at wavelength 1064 nm, m	7.95×10^{-9}	22,23	14.13×10^{-9}	22,23

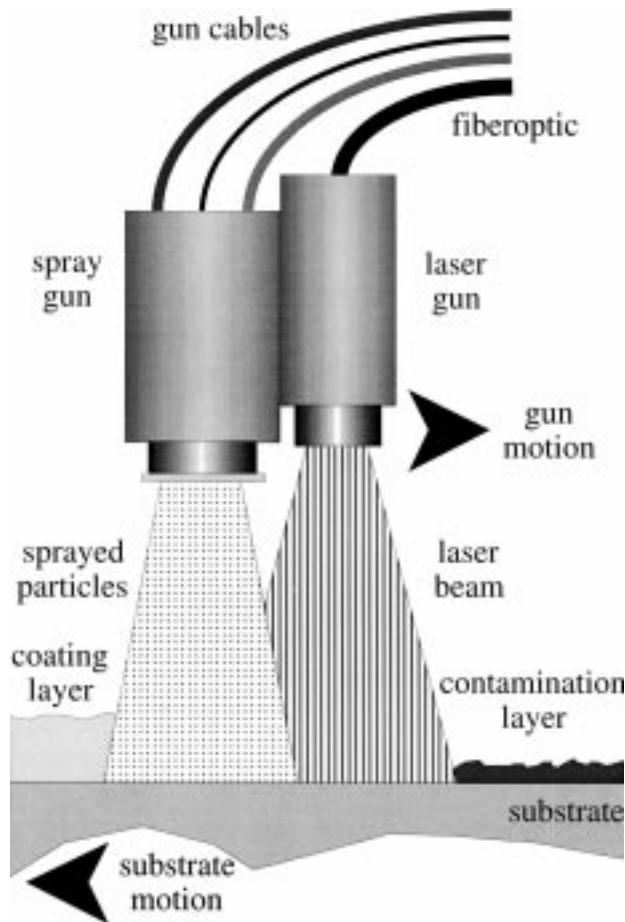


Fig. 2 Schematic principle of the PROTAL process

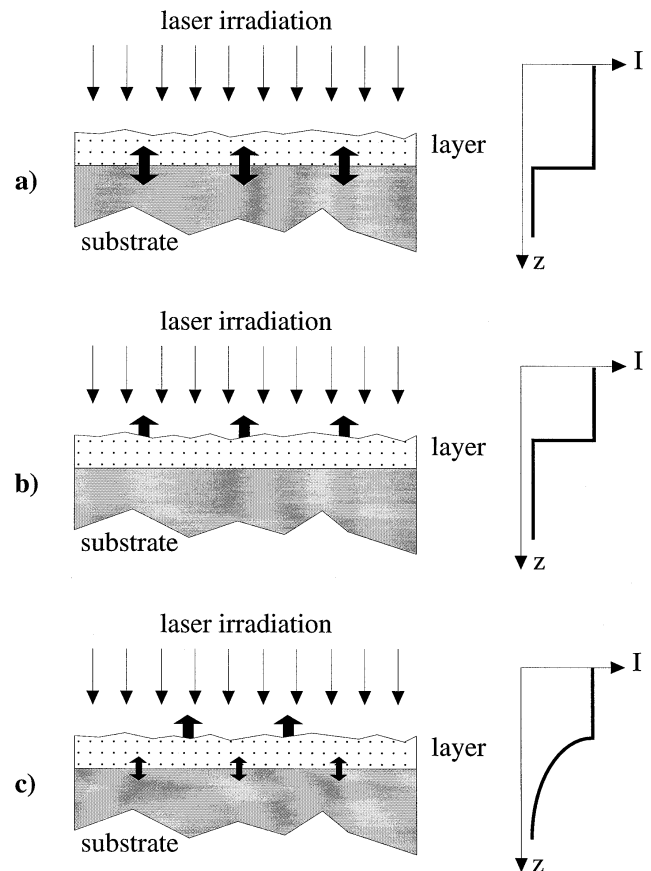


Fig. 3 Mechanisms of photonic absorption, where I represents the irradiation intensity and z the thickness. (a) Case of a transparent layer. (b) Case of an opaque layer. (c) Case of a half-transparent layer

atoms or molecules accumulate on this surface and modify its properties. This phenomenon is known as adsorption. Depending on the adsorption energy, it is possible to distinguish (Ref 11) physisorption (energy in the order of 0.1 eV), which is driven by Van der Waals type interaction and is schematically represented by the Morse potential curve (Ref 12), from chemisorption (energy between 0.1 and a few eV), which induces chemical bonds. When the energy delivered by laser irradiation becomes higher than the adsorption energy, the inverse phenomenon, named desorption, occurs.

The interaction between a laser beam and matter is a complex process that depends on (Ref 13-14), among other parameters, the substrate nature, the chemical and physical surface properties, the surface microgeometry, the beam energy density, the duration of irradiation, and the nature and pressure of the surrounding atmosphere. Schematically, the laser energy is absorbed following two complementary mechanisms (Ref 15), namely the photonic absorption and the inverse Bremsstrahlung absorption. In both cases, the final result induces the excitation of electrons in the matter. Then the relaxation of these electrons follows three different mechanisms, depending on the electric properties of the irradiated matter. For insulating materials, there is trapping of the excited electrons. For semiconductor materials, the relaxation is accomplished by heat radiation. Finally, for metallic materials (which is the most often encountered case in surface preparation for thermal spraying), the relaxation passes by the emission of a quantum of vibration energy (i.e., phonon). In such a way, the phenomenon will consist of either thermal effects (the irradiation absorption increases the temperature locally until vaporization phenomena occur) or nonthermal effects such as photoablation (Ref 16). In every case, for each material, an intensity threshold is observed (Ref 17-18). When the intensity is low, the vaporization of the matter is practically nonexistent, and energy is consumed to activate chemical mechanisms. When the intensity reaches intermediate values, an important substrate vaporization occurs (but emitted vapors remain transparent to the laser irradiation). For high values of intensity, the same phenomenon occurs, except that emitted vapor becomes opaque to the laser irradiation, which is very quickly absorbed, forming a plasma.

2.2 Laser Ablation

The laser ablation behavior brings together the aforementioned phenomena. The cleaning of a contaminated substrate implementing laser ablation leads to a surface free of organic components and oxide layers. Parameters to be chosen depend mainly on the nature of the contamination (Fig. 3) (Ref 19). If the contamination is transparent to the laser beam, the intensity is adsorbed by the substrate (the thermal thickness, which is the thickness into which the heat is contained, depends on the nature of the material; for metallic substrate, it varies usually between 0.2 and 0.5 μm). The thermal effect abruptly dilates the surface and induces the breaking and ejection of the contamination layers. If the contamination layer is opaque to the laser beam, the same phenomena occur, but inside the layer. Finally, if pollutants are half-transparent to the irradiation, intermediate phenomena (absorption by both the layers and the substrate) occur. Moreover, and as already mentioned, the laser ablation process is a threshold process; that is, ablation occurs if the energy is

higher than a given threshold. This threshold depends on the nature of the matter, as schematically presented in Fig. 4. Depending on the laser processing parameters, a selective ablation of either the greases; the greases and the oxide layers; or the greases, the oxide layers, and the substrate material can be obtained.

3. Laser/Substrate Interaction

Control of the laser/substrate interaction is a key point regarding the PROTAL process. The laser irradiation parameters have to be selected depending on the substrate nature. Two substrates exhibiting significantly different physical characteristics and for which surface preparation prior to thermal spraying implementing conventional techniques (e.g., grit blasting) are critical were selected as examples: 2017 aluminum-base alloy and Ti-6Al-4V titanium-base alloy.

3.1 Surface Temperature

Depending on the thermal and optical characteristics of the substrates (Table 1) (Ref 14, 20-23), different phenomena, such as heating, roughening, and ablation, can be observed according to the energy density of the beam and the interaction time. To investigate the occurrence of these transformations during the laser-matter interaction, experiments were first carried out without the plasma spraying stage.

Initially, temperature evolution of the substrate surface with respect to time was estimated for several specific average power densities using a simple mathematical modeling considering only the temperature effect (Ref 24). Assuming physical properties of the materials and absorbability independent from temperature, the temperature at location, z , and at time, t , $[\Delta T(z, t)]$ is expressed as:

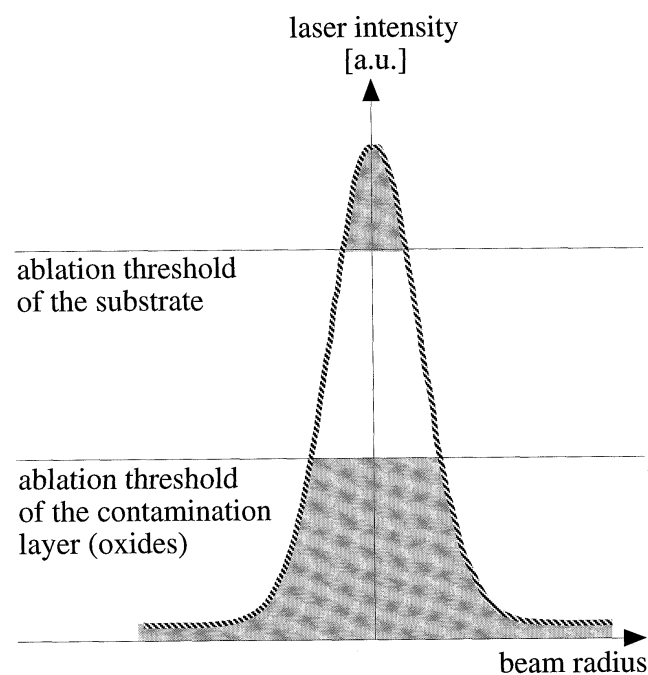


Fig. 4 Principle of the laser ablation process

$$\Delta T(z,t) = \frac{2 \cdot E_0 \cdot A \cdot \sqrt{\chi}}{k} \cdot \left[\sqrt{t} \cdot \text{ierfc} \left(\frac{z}{2 \cdot \sqrt{\chi \cdot t}} \right) - (t > t_p) \sqrt{(t - t_p)} \cdot \text{ierfc} \left(\frac{z}{2 \cdot \sqrt{\chi \cdot (t - t_p)}} \right) \right] \quad (\text{Eq 1})$$

where E_0 is the energy density, $\text{J} \cdot \text{m}^{-2}$; A is the absorptivity, %; χ is the thermal diffusivity, $\text{m}^2 \cdot \text{s}^{-1}$; k is the thermal conductivity, $\text{W} \cdot \text{m}^{-1} \cdot \text{K}^{-1}$; t is the interaction time, s; z is the depth location, m; and t_p is the irradiation duration, s. The $\text{ierfc}(x)$ function is defined as:

$$\text{ierfc}(x) = \int_x^\infty \text{erfc}(\zeta) d\zeta = \frac{1}{\sqrt{\pi}} e^{-x^2} - x \cdot \text{erfc}(x) \quad (\text{Eq 2})$$

$$\text{erfc}(x) = 1 - \text{erf}(x) = \frac{2}{\sqrt{\pi}} \int_x^\infty e^{-\zeta^2} d\zeta \quad (\text{Eq 3})$$

As an example, results are presented for a 2017 aluminum-base alloy substrate (Fig. 5). During the first 10 ns (corresponding to the irradiation duration), a progressive increase of the temperature can be observed, and for an energy density over $1.5 \text{ J} \cdot \text{cm}^{-2}$, melting of the material can occur. In fact, not all of the power of the beam will convert into heat within the substrate, particularly due to absorption effects by the vaporized material after a few nanoseconds.

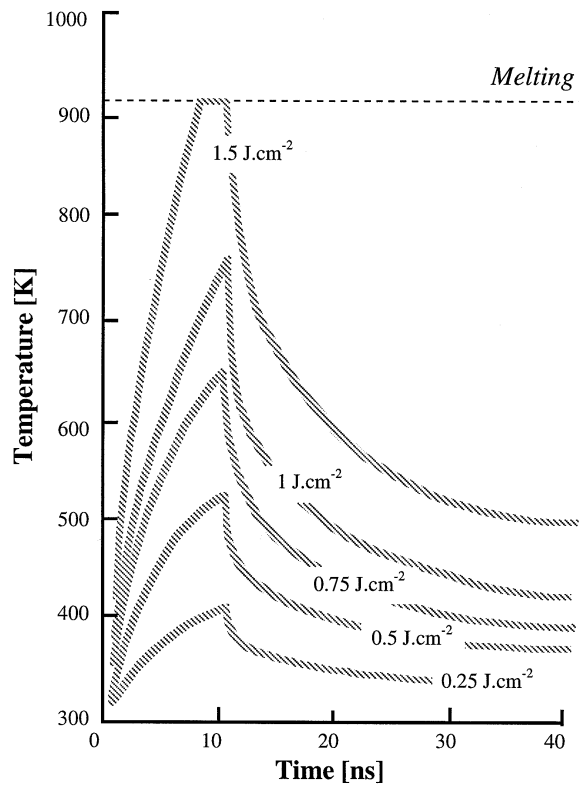
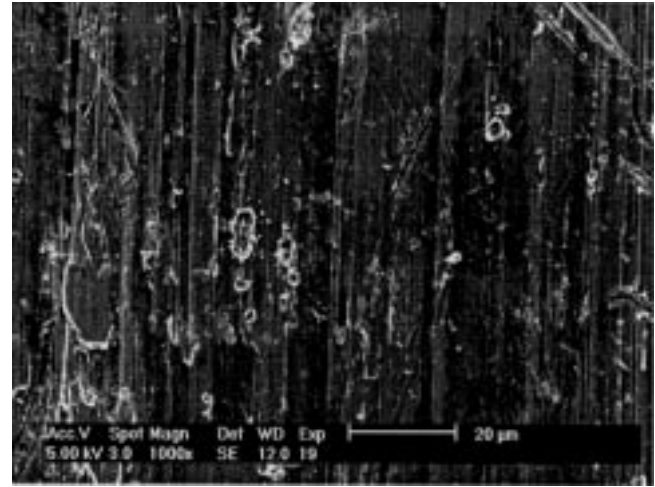


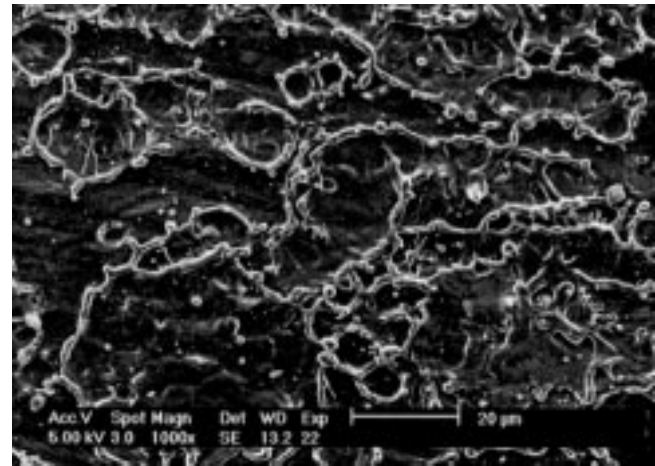
Fig. 5 Computed surface temperature evolution versus time for a 2017 aluminum-base alloy substrate

3.2 Surface Morphology versus Energy Density

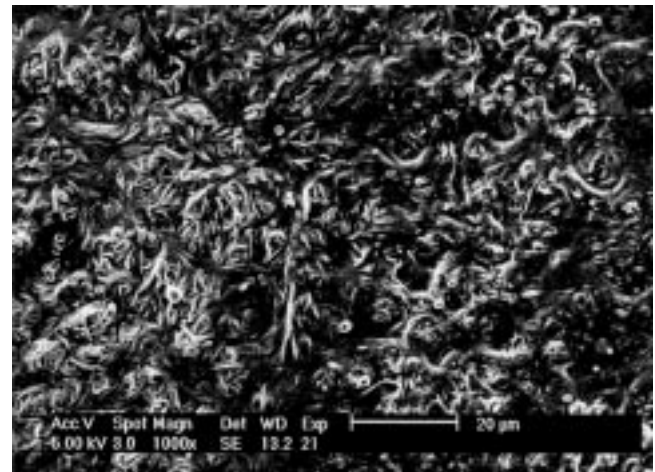
Several mechanisms, such as plasma extension and shock waves, can lead to a modification of the surface microgeometry



(a)



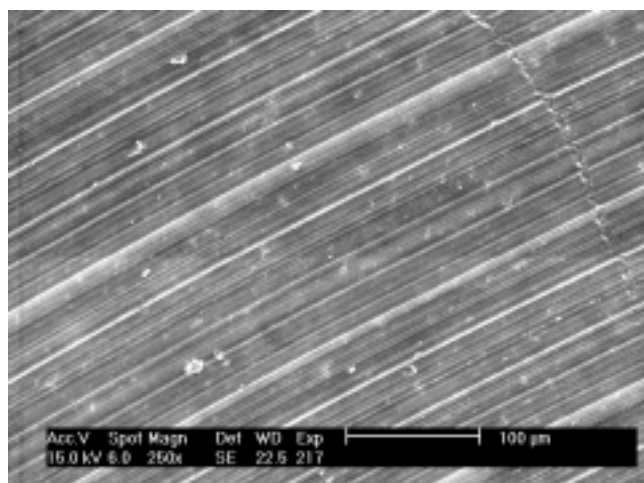
(b)



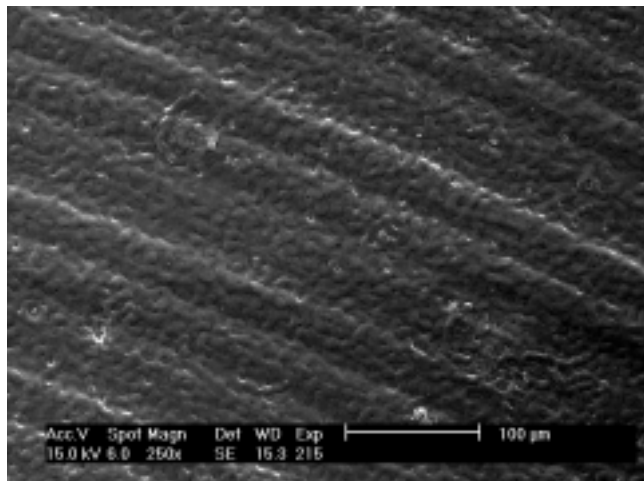
(c)

Fig. 6 Scanning electron microscopy observations of a 2017 aluminum-base alloy substrate for different energy densities. (a) $1 \text{ J} \cdot \text{cm}^{-2}$, (b) $2 \text{ J} \cdot \text{cm}^{-2}$, (c) $3 \text{ J} \cdot \text{cm}^{-2}$

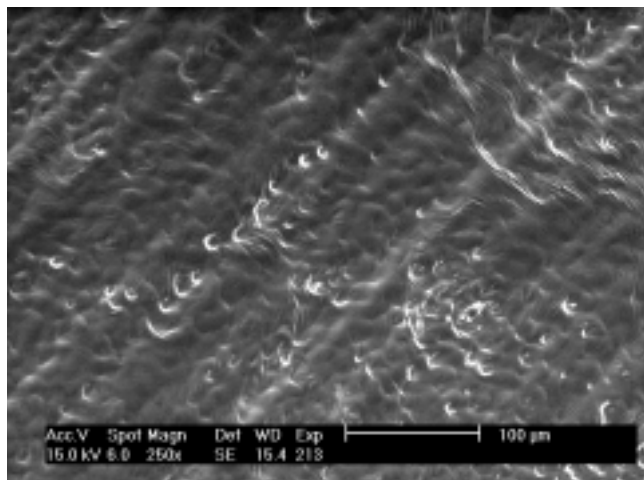
(Ref 15-18) during laser irradiation. Scanning electron microscopic (SEM) observations (Fig. 6-7) and laser surface profilometry measurements (Fig. 8) were performed on the



(a)



(b)



(c)

Fig. 7 Scanning electron microscopy observations of a Ti-6Al-4V titanium-base alloy substrate for different energy densities. (a) $1 \text{ J} \cdot \text{cm}^{-2}$. (b) $2 \text{ J} \cdot \text{cm}^{-2}$. (c) $3 \text{ J} \cdot \text{cm}^{-2}$

substrate material after laser irradiation for several energy densities. Results reveal a strong dependence of the surface morphology with respect to the physical characteristics of the material. A preferential laser-matter interaction appears around pores for the 2017 aluminum alloy until a total modification of the surface is induced. Concerning the Ti-6Al-4V titanium alloy, plastic deformation can be observed with an increase in the energy density of the laser. Thus, a significant roughness increase can be noted from $1.5 \text{ J} \cdot \text{cm}^{-2}$ for the aluminum-base alloy, while this effect starts earlier but remains moderate in the case of the titanium alloy substrate. Physical characteristics of the material can then induce strong different behaviors during laser irradiation (Ref 25).

4. Deposition on an Aluminum-Base Substrate

4.1 Materials

A 2017 aluminum-base alloy (in weight percent, 0.5Si-4Cu - 0.7Mn-0.6Mg-0.7Fe-0.1Cr, bal Al) was chosen to perform the

Table 2 Feedstock materials characteristics

Feedstock	Manufacturer reference	Composition, wt%	Particle size distribution, μm
Pure copper	AMDRY 3269	Copper, 99.9	-90 + 45
Nickel-chromium	AMDRY 4535	Nickel, 80 Chromium, 20	-45 + 5
Grey alumina	AMDRY 6226	Alumina, 87 Titania, 13	-45 + 22

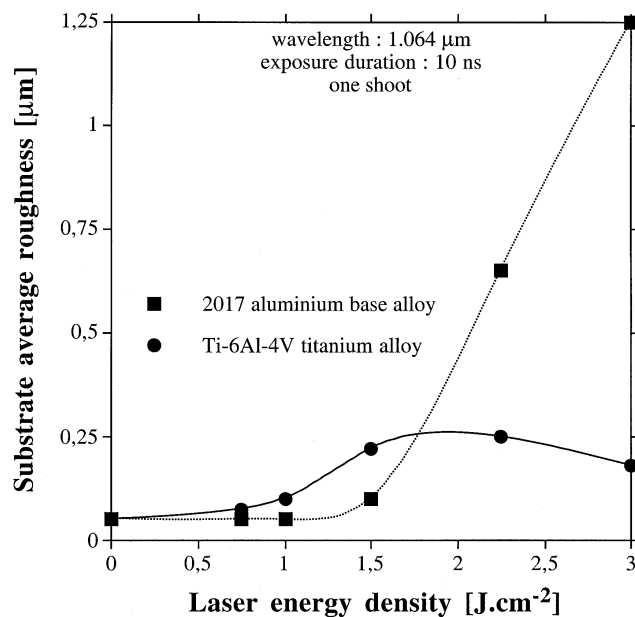


Fig. 8 Evolution of average surface roughness versus laser energy density, for 2017 aluminum and Ti-6Al-4V substrates

deposition experiments. Specimens were buttons 25 mm in diameter and 10 mm in thickness.

Several feedstock materials were considered in this study, namely two metallic (e.g., pure copper AMDRY 3269 and 80Ni-20wt%Cr AMDRY 4535) and a ceramic powder (e.g., gray alumina 87Al₂O₃-13wt%TiO₂ AMDRY 6226), shown in Table 2.

4.2 Processing Parameters

The Nd:YAG laser source used for this study had an average power of 100 W. The system was designed to be added to existing equipments (i.e., plasma guns and high velocity oxyfuel guns), without modifying spraying parameters (e.g., processing parameters and kinetic parameters). The laser beam was guided from the laser cavity to the laser gun by fiberoptics, permitting good flexibility of the system. As displayed on Fig. 9, the beam profiles at the exit of a fiberoptic are characterized by “top-hat” distributions, thereby allowing homogeneous treatment of the irradiated surfaces. The beam focal point of the laser was located above the sample surface, so the resulting laser energy density, ED ($J \cdot m^{-2}$), on the treated surface is defined as:

$$ED = \frac{P}{\pi \cdot r^2 \cdot s} \quad (\text{Eq 4})$$

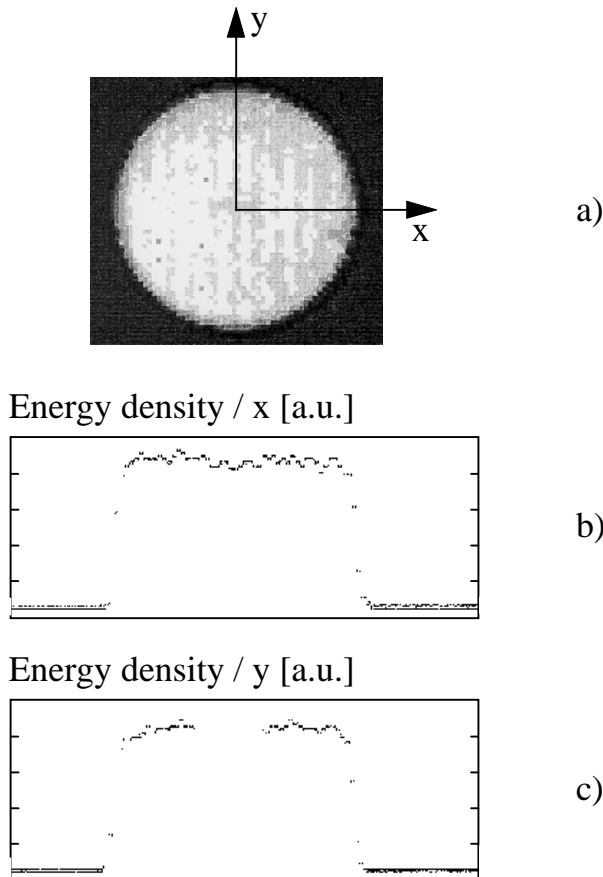


Fig. 9 “Top-hat” beam profile at the exit of a fiber optic. (a) Spatial distribution. (b) Radial distribution/x. (c) Radial distribution/y

where P is the laser average power, W; r is the laser spot radius on the substrate surface, m^2 ; and s is the frequency repetition rate, s^{-1} . The laser torch and the plasma torch were installed on a robot head, and specimens were mounted on a rotating sample holder. The coating was classically produced by several passes in front of the system. Spray parameters were close to standard spray parameters, listed in Table 3. The relative gun/substrate velocity was slightly adjusted depending on the choice of the laser energy density. The powder feed rate and the number of passes were adapted to obtain an average value of comparable coating thicknesses, in the range of 400 μm .

4.3 Interfacial Indentation Test

Coating adhesion was estimated by implementing the interfacial indentation test (Ref 26-28), which permits local measurements compared to the standard ASTM C 633-79 tensile adhesion test (TAT) (Ref 29). Applying a Vickers indenter is one method of pulling the coating from the substrate and hence developing a semicircular crack at the interface, the length of which depends on the quality of interface adhesion. The hypothesis of crack growth governed by mode I opening was made (Ref 26), and the hardness relation can be used to determine the interfacial toughness K_{Ic} as:

$$K_{Ic} = \frac{1}{\pi^{3/2} \cdot \tan \psi} \cdot \frac{P}{C^{3/2}} \quad (\text{Eq 5})$$

where P is the load, N; C the crack length, m; ψ is the indenter half summit angle, 68° . The K_{Ic} ($Pa \cdot m^{-1/2}$) can be considered as a mechanical characteristic of the interface even if it is influenced by the Young's modulus and thickness of the coating. Each given value is the average of ten measurements.

4.4 Tensile Adhesion Test

Tensile adhesion tests were performed according to ASTM C 633-79 practice code using an HTK ultra-bond 100 glue (HTK, Hamburg, Germany).

5. Coating Adhesion

In order to compare the PROTAL process to the standard surface preparation techniques, a first group of samples was prepared using conventional surface preparation (i.e., degreasing

Table 3 Spray parameters

Feedstock	Nickel-		
	Pure copper, AMDRY 3269	chromium, AMDRY 4535	Grey alumina, AMDRY 6226
Powder feed rate, $g \cdot min^{-1}$	25	25	25
Spray distance, mm	140	140	125
Argon primary plasma gas flow rate, $NL \cdot min^{-1}$	50	45	40
Hydrogen primary plasma gas flow rate, $NL \cdot min^{-1}$	6	10	14
Current, A	600	580	530
Relative velocity, $m \cdot min^{-1}$	46	46	46

and sand blasting, group 1), and a second group was treated with the PROTAL process (group 2).

5.1 Coating/Substrate Interface

Considering the coating-substrate interface (Fig. 10), it appears that the interface of the sample corresponding to the PROTAL process is clear and smooth, whereas the interface of the sand-blasted sample is irregular and rough, as usual. The samples treated by the PROTAL process were taken directly from the machine shop and manipulated barehanded; that is, no special clean handling operations were taken.

5.2 Coating Adhesion

Significant differences were observed between the different treatments both with the interfacial indentation test (Fig. 11) and the tensile adhesion test (Fig. 12). For a given coating/substrate system, the interfacial indentation and the tensile adhesion tests produced similar values for the PROTAL and standard processes. Meanwhile, the interfacial indentation conditions seemed, generally speaking, more favorable for the PROTAL process while the tensile adhesion test favored the standard process. These results clearly show the effectiveness of the PROTAL process together with a strong influence of the material properties on the laser treatment. Due to the mechanical or thermo-physical characteristics of the different coatings or of the substrate, the laser impact can be different, and therefore pa-

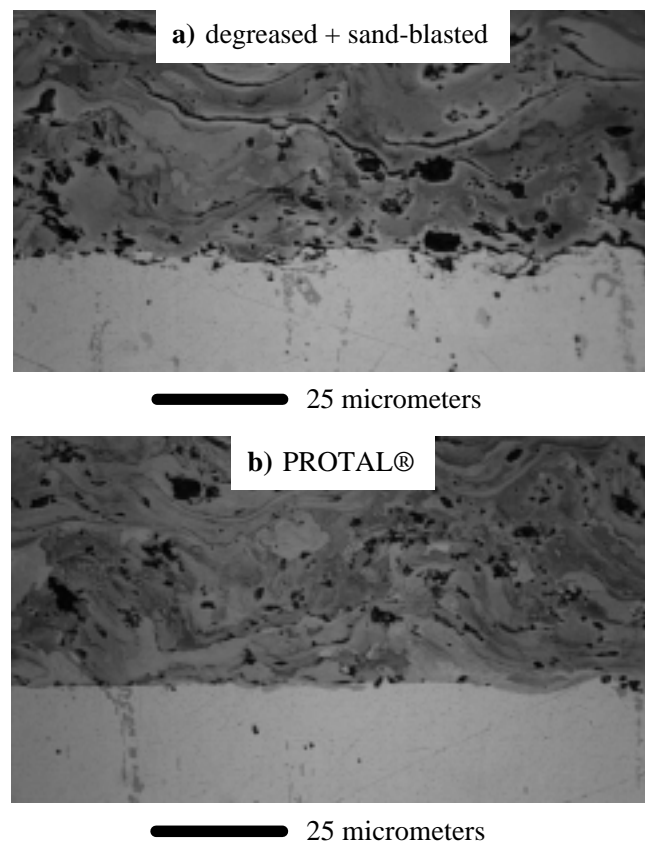


Fig. 10 Pure copper coating onto a 2017 aluminum-base alloy substrate. (a) Degreased and grit-blasted sample. (b) PROTAL process

rameters should be adjusted. A further optimization of the laser processing parameters should then permit enhanced results as already shown with other systems (Ref 1).

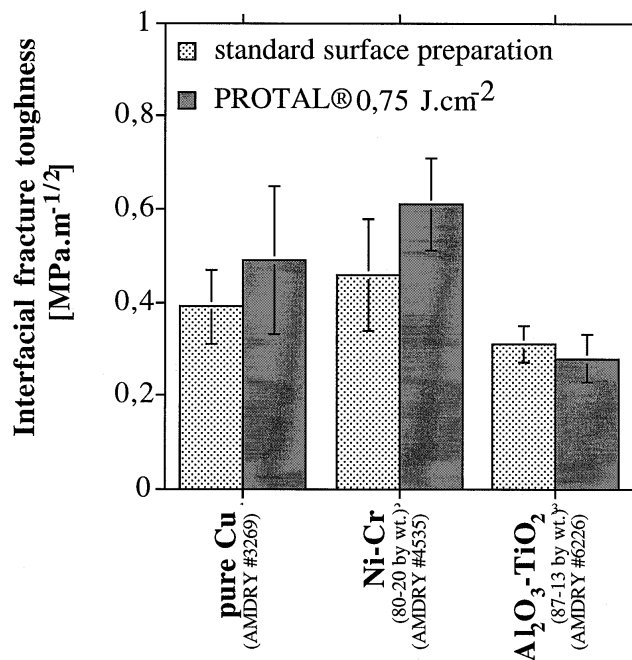


Fig. 11 Comparison of interfacial toughness for different coatings on an aluminum-base substrate implementing classical surface preparation and PROTAL process with an energy density of $0.75 \text{ J} \cdot \text{cm}^{-2}$

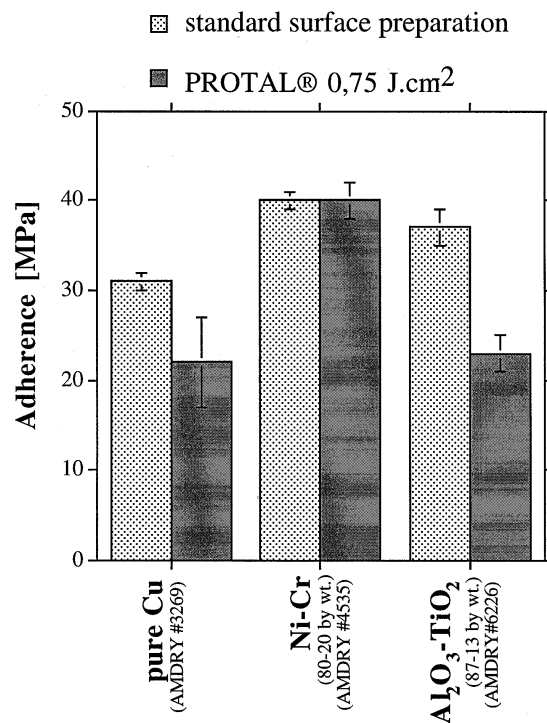


Fig. 12 Comparison of adherence from tensile adhesion tests for different coatings on an aluminum-base substrate implementing classical surface preparation and PROTAL process with an energy density of $0.75 \text{ J} \cdot \text{cm}^{-2}$

6. Conclusions

The PROTAL process, implementing laser technology in conjunction with the spraying process, is a technique able to replace actual surface preparation procedures before spraying. It permits not only the elimination of pollutants (e.g., greasy substances, oxide layers, and dusts), but it also generates good bonding of the coating to the substrate. The process is performed in a single step with spraying and should thus, among other advantages, improve the overall quality of thermal spray coatings and reduce their global cost.

Acknowledgment

This work was supported by the European Community under grant program Eureka EU1472.

References

1. S. Audisio, M. Caillet, A. Galerie, and M. Mazille, Préparation d'une Surface (Surface Preparation), *Traitements de Surface et Protection contre la Corrosion (Surface Treatments and Protection against Corrosion)*, Les Éditions de Physiques, Paris, France, 1987, p 169-174
2. J. Wigren, Grit Blasting as Surface Preparation before Plasma Spraying, *Surf. Coat. Technol.*, Vol 34, 1988, p 101-108
3. H. Gray, L. Wagner, and G. Lütjering, Influence of Surface Treatment on the Fatigue Behavior of Ti-Alloys at Room and Elevated Temperatures, *Sixth World Conference on Titanium*, P. Lacombe, R. Tricot, and G. Béanger, Ed., Les Éditions de Physique, Paris, France, 1998, p 1895-1900
4. R.A. Jukes, The Fatigue Properties of a High Strength Titanium Alloy, *The Science, Technology and Application of Titanium*, R.I. Jaffee and N.E. Promisel, Ed., Pergamon Press, 1970, p 923-931
5. T.A. Taylor, Surface Roughening of Superalloys by High Pressure Pure Waterjet, *Thermal Spray Science and Technology*, C.C. Berndt and S. Sampath, Ed., ASM International, 1995, p 351-358
6. J.K. Knapp and T.A. Taylor, Waterjet Roughened Surface Analysis and Bond Strength, *Surf. Coat. Tech.*, Vol 86-87, 1996, p 22-27
7. N. Iwamoto, Y. Makino, N. Umesaki, S. Endo, and H. Kobayashi, The Effects of Pretreatments of Metals on Bond Adhesion, *10th International Thermal Spraying Conference Proceedings*, Deutscher Verlag für Schweißtechnik GmbH, Düsseldorf, Germany, 1983, p 18-20
8. O.O. Popoola and M.J. Zaluzsec, Mechanical and Chemical Modifications of Cast Aluminum Alloy Surfaces by E.D.M. for Thermal Spray Coating Adhesion, *Thermal Spray: Practical Solutions for Engineering Problems*, C.C. Berndt, Ed., ASM International, 1996, p 968
9. C. Coddet and T. Marchione, Procédé de Préparation et de Revêtement de Surface et Dispositif pour la Mise en Oeuvre Dudit Procédé (Process for the Preparation and Coating of a Surface and Apparatus for Practicing Said Process), French Patent FR9209277, 21 July 1993
10. C. Coddet and T. Marchione, Process for the Preparation and Coating of a Surface and Apparatus for Practicing Said Process, Canadian and U.S. Patent extensions
11. D. Spanjaard, "Présentation de la Surface" (Presentation of the Surface), École Thématique du CNRS sur l'Ablation Laser (CNRS Meeting on Laser Ablation), CNRS, 1996, p 77-111
12. J.C. Mallet and R. Fourmié, *Cours de Chimie (A Course on Chemistry)*, Dunod, Paris, 1995, p 547
13. M. Bouchy and J.C. André, Processus Primaires en Photochimie et Photophysique (Elementary Processes in Photochemistry and Photophysics), *Techniques d'Utilisation des Photons (Techniques for Using Photons)*, J.C. André and A.B. Vannes, Ed., DOPEE Diffusion, Avon, France, 1992, p 67-95
14. A. Catherinot, D. Damiani, C. Champeaux, and G. Girault, Photoablation par Laser (Laser Photoablation), *Laser de Puissance et Traitements des Matériaux (Power Laser and Materials Treatments)*, Presses Polytechniques et Universitaires Romandes, Lausanne, Switzerland, 1991, p 19-57
15. L. Landau and E. Lifchitz, *Physique Statistique (Statistical Physics)*, MIR Éditions, Moscow, 1984, p 592
16. G. Petite and P. Daguzan, L'Absorption de l'Énergie et ses Conséquences (Energy Absorption and Its Consequences), *École Thématique du CNRS sur l'ablation Laser (CNRS Meeting on Laser Ablation)*, CNRS, 1996, p 159-218
17. D. Bäuerle, *Laser Processing and Chemistry*, 2nd ed., Springer Verlag, 1996, p 649
18. B.N. Chichkov, C. Momma, S. Nolte, F. Von Alvensleben, and A. Tünnermann, Femtosecond, Picosecond and Nanosecond Laser Ablation of Solids, *Appl. Phys. A*, Vol 63, 1996, p 109-115
19. N.P. Leung, W. Zapka, and W. Ziemlich, Cleaning Techniques for Removal of Surface Particulates, *J. Appl. Phys.*, Vol 7, 1992, p 3515-3523
20. *Handbook of Chemistry and Physics*, 66th ed., R.C. Weast, Ed., CRC Press, Inc., 1986
21. *Metals Handbook, Desk Edition*, H.E. Boyer and T.L. Gall, American Society for Metals, 1985
22. A. Catherinot, Interaction Laser-Matériau, Aspects Thermiques/Nonthermiques, Photoablation et Transport de la Matière Ejectée, *Ecole Thématique du CNRS sur l'ablation Laser (CNRS Meeting on Laser Ablation)*, CNRS, 1996
23. M. Bass, *Handbook of Optics (Devices, Measurements and Properties)* Vol 2, 2nd ed., McGraw-Hill Inc., 1995
24. F. Mzali, "Etude des Effets d'une Irradiation de Surfaces Métalliques par un Laser ($\lambda = 1.064 \mu\text{m}$) de Courte Durée d'impulsion (10 ns)" (Study of the Effects of a Metal Surface Irradiation by Short Laser Pulses), LERMPS Internal Report, Institut Polytechnique de Sévenans, Belfort, France, 1997
25. A.B. Vannes, Effets Thermiques du Rayonnement Laser (Thermal Effects of Laser Beam), *Techniques d'Utilisation des Photons (Techniques for Using Photons)*, J.C. André and A.B. Vannes, Ed., DOPEE Diffusion, Avon, France, 1992, p 349-354
26. D. Choulier, P. Fluzin, G. Thauvin, and C. Coddet, Characterization of the Substrate—Coating Interface Toughness by the Interfacial Indentation Test. Influence of Different Parameters on the Bond Strength, *First Plasma-Technik Symposium (Lucerne, Switzerland)*, Vol 2, 18-20 May 1988, p 293-305
27. P. Ostojic and R. McPherson, Indentation Toughness Testing of Plasma Sprayed Coatings, *Materials Forum*, Vol 10 (No. 4), 1987
28. D. Choulier, P. Fluzin, and C. Coddet, Influence of Spraying Parameters on the Adherence of Atmospheric Plasma Sprayed Coatings, *Sixth International Conference of Heat Treatment of Metals (Chicago, IL)*, 28-30 Sept 1988, p 75-78
29. ASTM Designation C 633-79, Standard Test Method for Adhesion or Cohesive Strength of Flame-Sprayed Coatings, *1986 Annual Book of ASTM Standards*, Part 2, ASTM, 1986, p 754-760